Photon-proton and photon-photon scattering from nucleon-nucleon forward amplitudes

M. M. Block
Department of Physics and Astronomy, Northwestern University, Evanston, Illinois 60208

E. M. Gregores and F. Halzen
Department of Physics, University of Wisconsin, Madison, Wisconsin 53706

G. Pancheri
INFN-Laboratori Nazionali di Frascati, P.O. Box 13, I-00044 Frascati, Italy
(Received 16 September 1998; published 9 August 1999)

We show that the data on γp and $\gamma\gamma$ interactions can be derived from the pp and $\bar{p}p$ forward scattering amplitudes using vector meson dominance and the additive quark model. The nucleon-nucleon data are parametrized using a model where high energy cross sections rise with energy as a consequence of the increasing numbers of soft partons populating the colliding particles. We present detailed descriptions of the data on the total and elastic cross sections, the ratio of the real to imaginary part of the forward scattering amplitude, and the slope of the differential cross sections for pp, $\bar{p}p$, γp, $\gamma\gamma$, $\gamma p \to \gamma V$ and $\gamma\gamma \to V_i V_j$ reactions, where $V = \rho, \omega, \phi$. We make a wide range of predictions for future DESY HERA and CERN LHC experiments and for $\gamma\gamma$ measurements at CERN LEP. [S0556-2821(99)00717-1]

PACS number(s): 11.80.Fv, 12.38.Lg, 13.60.Hb

I. INTRODUCTION

We show that the data on γp and $\gamma\gamma$ interactions can be derived from the pp and $\bar{p}p$ forward scattering amplitudes using vector meson dominance (VMD) and the additive quark model. We first show that the data on the total cross section, the slope parameter B of the elastic differential cross section, and the ratio of the real to imaginary part of the forward scattering amplitude ρ for pp and $\bar{p}p$ interactions can be nicely described by a model where high energy cross sections grow with energy as a consequence of the increasing number of soft partons populating the colliding particles [1]. The differential cross sections for the Fermilab Tevatron and the CERN Large Hadron Collider (LHC) are predicted. Using this parametrization of the hadronic forward amplitudes we calculate the photoproduction cross sections, slope parameter B and ρ value from VMD and the additive quark model. We then obtain $\gamma\gamma$ cross sections which are parameter free, demonstrating the approximate validity of the factorization theorem using recent data from the CERN e^+e^- collider LEP.

All cross sections will be computed in an eikonal formalism guaranteeing unitarity throughout:

$$\sigma_{tot}(s) = 2\int \{1 - e^{-\chi_I(b,s)}\cos[\chi_R(b,s)]\}\, d^2\vec{b}. \qquad (1)$$

Here, χ is the complex eikonal ($\chi = \chi_R + i\chi_I$), and b is the impact parameter. The even eikonal profile function χ^{even} receives contributions from quark-quark, quark-gluon and gluon-gluon interactions, and therefore

$$\begin{aligned}\chi^{even}(s,b) &= \chi_{qq}(s,b) + \chi_{qg}(s,b) + \chi_{gg}(s,b) \\ &= i[\sigma_{qq}(s)W(b;\mu_{qq}) + \sigma_{qg}(s)W(b;\sqrt{\mu_{qq}\mu_{gg}}) \\ &\quad + \sigma_{gg}(s)W(b;\mu_{gg})], \qquad (2)\end{aligned}$$

where σ_{ij} are the cross sections of the colliding partons, and $W(b;\mu)$ their overlap function in impact parameter space, parametrized as the Fourier transform of a dipole form factor. This formalism is identical to the one used in ''mini-jet'' models [2], as well as in simulation programs for minimum-bias hadronic interactions such as PYTHIA and SYBILL.

In this model hadrons asymptotically evolve into black disks of partons. The parametrization of the rising cross section, asymptotically associated with gluon-gluon interactions, is simply parameterized by a normalization, an energy scale, and two parameters: μ_{gg} which describes the ''area'' occupied by gluons in the colliding hadrons, and $J(=1+\epsilon)$. Here, J is defined via the gluonic structure function of the proton, which is assumed to behave as $1/x^J$ for small x. It therefore controls the soft gluon content of the proton. The introduction of the quark-quark and quark-gluon terms allows us to adequately parametrize the data at all energies, since the ''size'' of quarks and gluons in the proton can be different. In the present context, this model represents a convenient parametrization of the pp and $\bar{p}p$ forward scattering amplitude.

The photoproduction cross sections are calculated from this parametrization assuming vector meson dominance and the additive quark model. For the probability that the photon interacts as a hadron (P_{had}), we use the value $P_{had} = 1/240$ which can be derived from vector meson dominance. Our results show that its value is indeed independent of energy. It is, however, uncertain by 20% because it depends on whether we relate photoproduction to π-nucleon or nucleon-nucleon data (in other words, πN and NN total cross sections only satisfy the additive quark model to this accuracy). Subsequently, following Ref. [3], we obtain γp cross sections from the assumption that, in the spirit of VMD, the photon is a 2 quark state in contrast with the proton which is a 3 quark state. The γp total cross section is obtained from the even

eikonal for pp and $\bar{p}p$ by the substitutions $\sigma_{ij} \to \frac{2}{3}\sigma_{ij}$ and $\mu_i \to \sqrt{\frac{3}{2}}\mu_i$.

We will thus produce a parameter-free description of the total photoproduction cross section, the phase of the forward scattering amplitude and the forward slope for $\gamma p \to Vp$, where $V=\rho,\omega,\phi$. Interestingly, our results on the phase of $Vp \to Vp$ are in complete agreement with the values derived from Compton scattering results ($\gamma+p \to \gamma+p$) using dispersion relations. We also calculate the total elastic and differential cross sections for $\gamma p \to Vp$. This wealth of data is accommodated without discrepancy.

The $\gamma\gamma$ cross sections are derived following the same procedure. We now substitute $\sigma_{ij} \to \frac{4}{9}\sigma_{ij}$ and $\mu_i \to \frac{3}{2}\mu_i$ into the nucleon-nucleon even eikonal, and predict the total cross section and the differential cross sections for all reactions $\gamma\gamma \to V_iV_j$ at a variety of energies, where $V=\rho,\omega,\phi$.

The high energy $\gamma\gamma$ total cross section [4] has been measured by two experiments at LEP. While these measurements yield new information on its high energy behavior at center-of-mass energies in excess of $\sqrt{s}=15$ GeV, they may represent the last opportunity to measure the $\gamma\gamma$ cross section, and the two data sets appear to disagree. However, it has been argued that the original data are consistent within the errors [5] and that the observed disagreements are due to two different Monte Carlo programs used to extract the quoted values. We here point out that our analysis nicely accommodates the L3 result [6]. Our model approximately satisfies the factorization theorem, $\sigma_{pp}/\sigma_{\gamma p}=\sigma_{\gamma p}/\sigma_{\gamma\gamma}$, because of its small eikonal. The OPAL data do not satisfy it. In fact, no model incorporating the additive quark model and factorization can accommodate the OPAL data. VMD and factorization are sufficient to prevent one from adjusting P_{had}, or any other parameters, to change this conclusion.

An interesting theoretical issue emerges when it is noticed that we applied the additive quark model to the full hadronic eikonal, not just to the quark subprocesses. This was not a choice; the data clearly enforce it. For example, if we do not apply the quark counting rules to the gluon-gluon subprocess, the model fails to reproduce the forward slope of the $\gamma p \to \gamma V$ reactions and the ratio of the imaginary to real part of the $\gamma p \to \gamma p$ forward amplitude. It, in fact, fails dramatically. The result may suggest a structure of the nucleon where the gluons cluster around the original valence quarks, as in the valon model [7]. This picture is reinforced by correlation measurements between quarks and gluons, derived from the observation of multiple parton final states in hadron collisions [8].

II. HIGH ENERGY PROTON-PROTON AND PROTON-ANTIPROTON SCATTERING

In this section we discuss our QCD-inspired parametrization of the forward amplitudes. To determine its parameters, we fit all high energy forward $\bar{p}p$ and pp scattering data above 15 GeV, for the total cross section (σ_{tot}), the ratio of the real to the imaginary part of the forward scattering amplitude (ρ), and the logarithmic slope of the differential elastic scattering cross section in the forward direction (B).

TABLE I. Value of the parameters used in the fit.

Fixed	Fitted
$m_0=0.6$ GeV	$C=5.42\pm0.16$
$\epsilon=0.05$	$C_{qq}^{log}=0.167\pm0.037$
$\mu_{qq}=0.89$ GeV	$C'_{gg}=(1.03\pm0.12)\times10^{-3}$
$\mu_{gg}=0.73$ GeV	$C_{Regge}^{even}=28.8\pm2.0$
$\mu_{odd}=0.53$ GeV	$C_{odd}=7.55\pm0.30$
$\alpha_s=0.5$	$s_0=10.3\pm0.88$ GeV^2

Then, we compare the experimental data for the elastic scattering cross section and for the differential elastic scattering with our results. Finally, a prediction is made for the differential elastic scattering at the LHC.

Our QCD-inspired parametrization satisfies crossing symmetry; i.e., it is either even or odd under the transformation $E \to -E$, where E is the laboratory energy. This allows us to simultaneously describe $\bar{p}p$ and pp scattering. It also satisfies analyticity and unitarity because of the eikonal formalism. Since the total cross section asymptotically rises as $\log^2 s$, our QCD-inspired parametrization complies with the Froissart bound. The eikonal formalism for calculating σ_{tot}, ρ and B is given in Appendix A. Details of the analyticity, the Froissart bound, and the QCD-inspired eikonal are given in Appendix B.

The even part of our QCD-inspired eikonal contains quark-quark, quark-gluon and gluon-gluon components. The gluon-gluon component dominates at high energy and depends on ϵ, μ_{gg}, a threshold mass m_0, and a normalization C'_{gg}. The quark-quark and quark-gluon interactions are parametrized by μ_{qq} and by terms which are constant, Regge behaved, and logarithmic as a function of the energy.

In all 11 parameters are used, and their values are presented in Table I. The low energy region, where the differences between $\bar{p}p$ and pp scattering are substantial, largely determines the 7 parameters necessary to fit the odd eikonal and the quark-quark and quark-gluon contribution to the

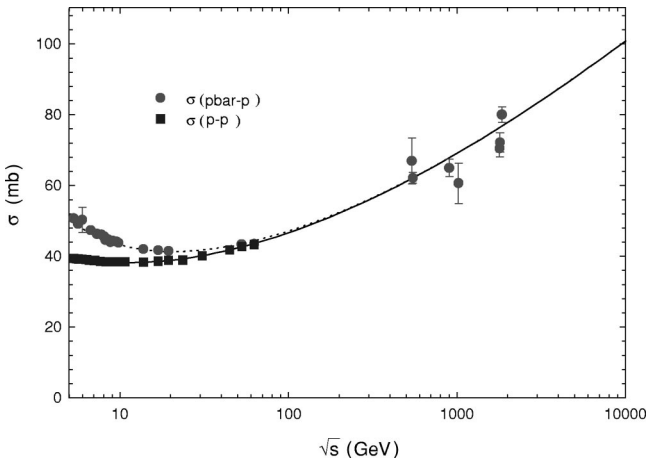

FIG. 1. The total cross section for pp and $\bar{p}p$ scattering. The solid line and squares are for pp and the dotted line and circles are for $\bar{p}p$.

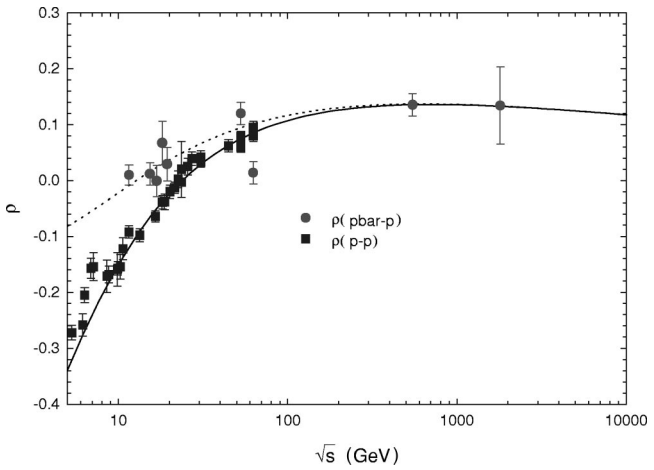

FIG. 2. The ratio of the real to imaginary part of the forward scattering amplitude for pp and $\bar{p}p$ scattering. The solid line and squares are for pp and the dotted line and circles are for $\bar{p}p$.

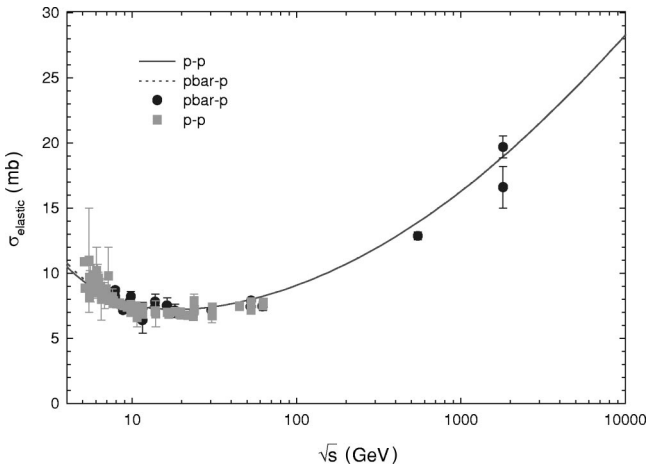

FIG. 4. Elastic scattering cross sections for pp and $\bar{p}p$ scattering. The solid line and squares are for pp and the dotted line and circles are for $\bar{p}p$.

even eikonal. Thus, they largely decouple from the high energy behavior. Hence, for $\sqrt{s} \gtrsim 25$ GeV, where the difference between $\bar{p}p$ and pp scattering becomes small, only 4 parameters are needed to describe all data.

We fit all the highest energy cross section data [E710 [9], Central Detector Facility (CDF) [10] and the unpublished Tevatron value [11]], which anchor the upper end of our cross section curves. The results of the fit are shown in Fig. 1. Data for ρ values and B are simultaneously fitted by our model in Figs. 2 and 3.

It can be seen from those figures that we obtain a satisfactory description of all 3 quantities, for both $\bar{p}p$ and pp scattering. The χ^2 of the fit is reasonably good (considering the large spread in some of the experimental data, as well as the discrepancies in the highest energy cross sections), giving a $\chi^2/N_{\mathrm{DF}} = 1.66$, for $N_{\mathrm{DF}} = 75$ degrees of freedom. From Fig. 2, we note that the fit to ρ is anchored at $\sqrt{s} = 550$ GeV by the very accurate measurement [12] of UA4/2 and passes through the E710 point [13]. The statistical uncertainty of the fitted parameters is such that at 25 GeV the cross section predictions are statistically uncertain to $\approx 1.3\%$, at 500 GeV are uncertain to $\approx 1.6\%$, and at 2000 GeV are uncertain to $\approx 2.5\%$.

In Fig. 4 we show the prediction for the elastic cross section along with the data for both $\bar{p}p$ and pp. The agreement is excellent. We note that $\sigma_{elastic}$ is rising more sharply with energy than the total cross section σ_{tot}. Comparing Fig. 1 with Fig. 4, we see that the ratio of the elastic to total cross section is rising with energy. The ratio is, of course, bounded by the value for the black disk [14,15], i.e., 0.5, as the energy goes to infinity.

Having fixed all parameters specifying our eikonal, we calculate $d\sigma/dt$, for various values of $\sqrt{s}$. The differential cross section at the Tevatron ($\sqrt{s} = 1800$ GeV) is shown in Fig. 5 along with E710 [16] data. The agreement over 4 decades is striking. The differential cross section for $\sqrt{s}$

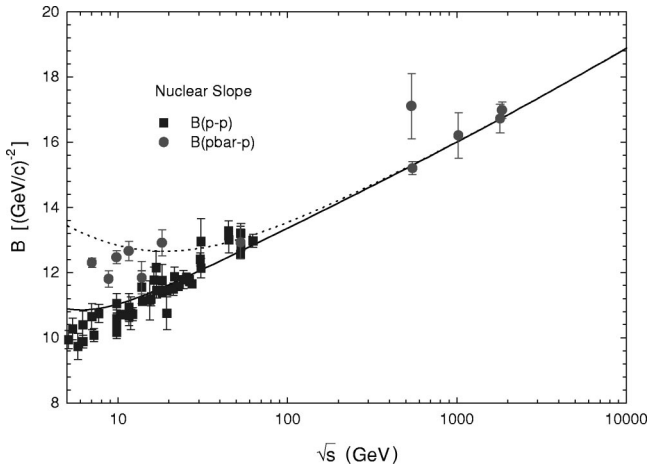

FIG. 3. The nuclear slope parameter for elastic pp and $\bar{p}p$ scattering. The solid line and squares are for pp and the dotted line and circles are for $\bar{p}p$.

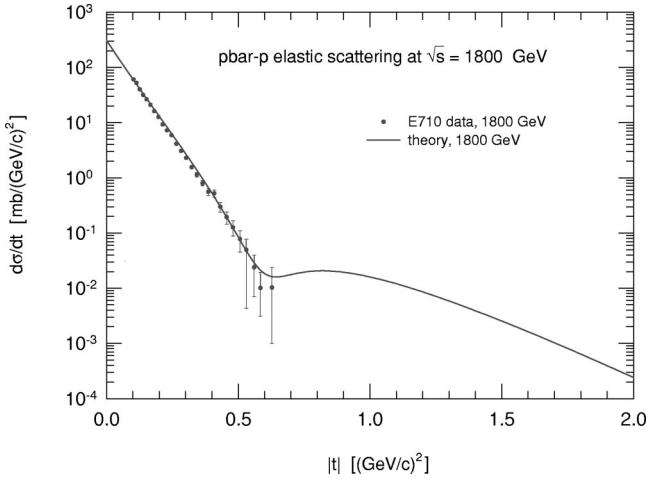

FIG. 5. The elastic differential scattering cross section for the reaction $\bar{p}p \to \bar{p}p$ at $\sqrt{s} = 1800$ GeV. The data points are from E710.

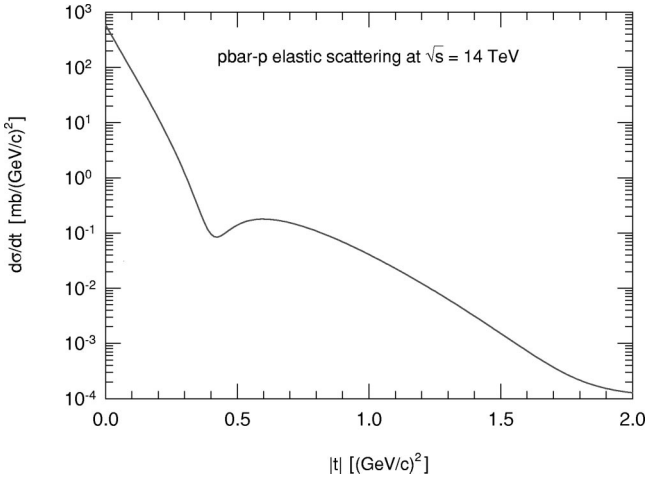

FIG. 6. The elastic differential scattering cross section for the reaction $\bar{p}p \to \bar{p}p$ at LHC.

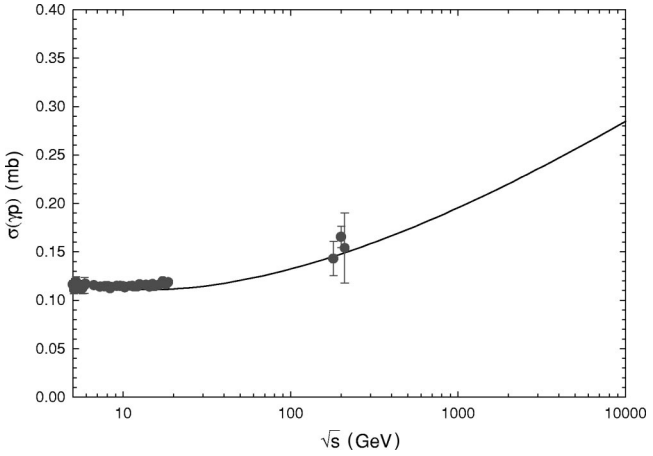

FIG. 7. The total cross section for γp scattering.

$=14$ TeV, the energy of the LHC, is plotted in Fig. 6. In particular, at small $|t|$, we predict that the curvature parameter C (see Appendix B for details) is negative. For energies much lower than 1800 GeV, the observed curvature has been measured as positive. For 1800 GeV, we see from Fig. 5 that the curvature parameter C is compatible with being zero. Block and Cahn [14,15] have pointed out that the curvature is predicted to go through zero near the Tevatron energy and that it should become negative thereafter. Asymptotically the proton approaches a black disk. Its curvature is always negative [14,15], $C=-R^4/192$, where R is the radius of the disk. Thus, the curvature has to pass through zero as the energy increases. ''Asymptopia'' is the energy region (energies much larger than the Tevatron) where the scattering approaches that of a sharp disk.

With the parameters we obtained from our fit, we predict the total cross section at the LHC (14 TeV) as $\sigma_{tot}=108.0 \pm 3.4$ mb, where the error is due to the statistical errors of the fitting parameters.

III. PHOTON-PROTON REACTIONS

We assume that the photon behaves like a two quark system when it interacts strongly. We therefore obtain γp scattering amplitudes by performing the substitutions $\sigma_{ij} \to \frac{2}{3}\sigma_{ij}$ and $\mu_i \to \sqrt{\frac{3}{2}}\mu_i$ in the even eikonal for nucleon-nucleon scattering, so that

$$\chi^{\gamma p}(s,b) = i[\tfrac{2}{3}\sigma_{qq}(s)W(b;\sqrt{\tfrac{3}{2}}\mu_{qq}) + \tfrac{2}{3}\sigma_{qg}(s)W(b;\sqrt{\tfrac{3}{2}\mu_{qq}\mu_{gg}}) + \tfrac{2}{3}\sigma_{gg}(s)W(b;\sqrt{\tfrac{3}{2}}\mu_{gg})]. \quad (3)$$

Using vector dominance, the photon-proton total cross section is then written as

$$\sigma_{tot}^{\gamma p}(s) = 2P_{had}\int \{1-e^{-\chi_I^{\gamma p}(b,s)}\cos[\chi_R^{\gamma p}(b,s)]\}\, d^2\vec{b}, \quad (4)$$

where P_{had} is the probability that a photon interacts as a hadron. We use the value $P_{had}=1/240$. This value is found by normalizing the total γp cross section to the low energy data, and is very close to that derived from vector dominance, 1/249. Using $f_\rho^2/4\pi=2.2$, $f_\omega^2/4\pi=23.6$ and $f_\phi^2/4\pi=18.4$, we find $\Sigma_V(4\pi\alpha/f_V^2)=1/249$, where $V=\rho,\omega,\phi$ (see Table XXXV, 393 of Ref. [17]).

With all eikonal parameters fixed by the nucleon-nucleon data, we can now calculate $\sigma_{tot}^{\gamma p}(s)$. The result is shown in Fig. 7. It reproduces the rising cross section for γp, using the parameters fixed by nucleon-nucleon scattering. This prediction only uses the 9 parameters of the even eikonal, of which only 4 are important in the upper energy region. The accuracy of our predictions are $\sim 1.5\%$, from the statistical uncertainty in our eikonal parameters.

We next consider the ''elastic'' scatterings

$$\gamma + p \to \rho_{virtual} + p \to \rho + p,$$
$$\gamma + p \to \omega_{virtual} + p \to \omega + p,$$
$$\gamma + p \to \phi_{virtual} + p \to \phi + p. \quad (5)$$

Here the photon virtually transforms into a vector meson which elastically scatters off of the proton. The strengths of these reactions is $\mathcal{O}(\alpha)$ times a strong interaction cross section. The true elastic cross section is given by Compton scattering on the proton, $\gamma + p \to \gamma + p$, which we can visualize as

$$\gamma + p \to \rho_{virtual} + p \to \rho + p \to \gamma + p,$$
$$\gamma + p \to \omega_{virtual} + p \to \omega + p \to \gamma + p,$$
$$\gamma + p \to \phi_{virtual} + p \to \phi + p \to \gamma + p. \quad (6)$$

It is clearly $\mathcal{O}(\alpha^2)$ times a strong interaction cross section, and hence is much smaller than ''elastic'' scattering of Eq. (5). Thus, we justify the use of Eq. (4) to calculate the total cross section, since only reactions with a photon in the final state are neglected.

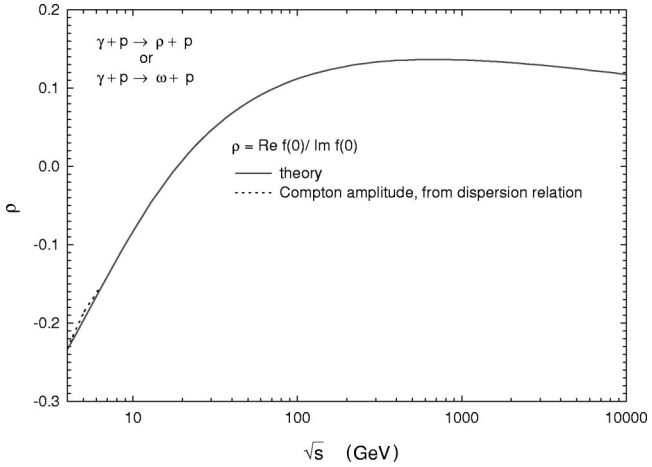

FIG. 8. Ratio of the real to imaginary part of the forward scattering amplitude for the ''elastic'' reactions $\gamma+p\rightarrow V_i+p$, where V_i is ρ^0, ω^0 or ϕ^0. The dotted curve is for Compton scattering from dispersion relations [18]. It has been slightly displaced from the solid curve for clarity in viewing.

We evaluate ρ and the slope B for the ''elastic'' scattering expressed in Eq. (5) using Eqs. (A12) and (A17). It can be seen from those equations that our predictions are free of P_{had} factors and are independent of normalization, it being the same for either $\rho p, \omega p$ or ϕp final states.

The dependence of ρ with the energy is shown in Fig. 8. Damashek and Gilman [18] have calculated the ρ value for Compton scattering on the proton using dispersion relations, i.e., the true elastic scattering reaction for photon-proton scattering. We compare this calculation, the dotted line in Fig. 8, with our prediction of ρ (the solid line). The agreement is so close that we had to move the two curves apart so that they may be viewed more clearly.

In Fig. 9 we show our results for the slope B as a function of the energy. The available experimental data for ''elastic'' ρp and ωp final states are also plotted. Again, the agreement of theory and experiment is very good.

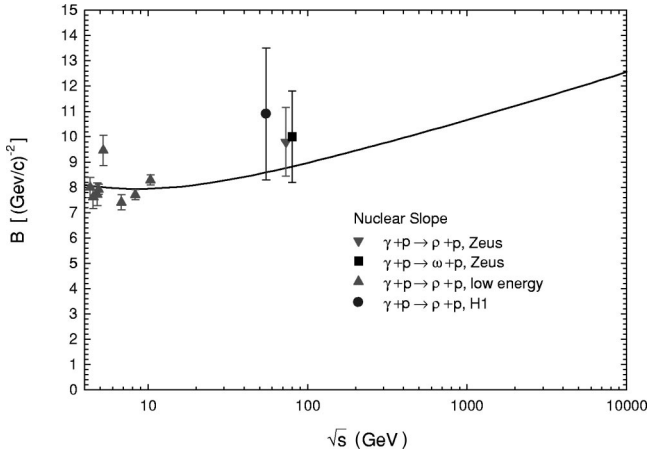

FIG. 9. Nuclear slope parameter for the ''elastic'' reaction $\gamma+p\rightarrow V_i+p$, where V_i is ρ^0, ω^0 or ϕ. For the reaction $\gamma+p\rightarrow\rho^0+p$, the inverted triangles are the Zeus data, the circles are the H1 data, and the triangles are the low energy data. For the reaction $\gamma+p\rightarrow\omega^0+p$, the squares are the Zeus data.

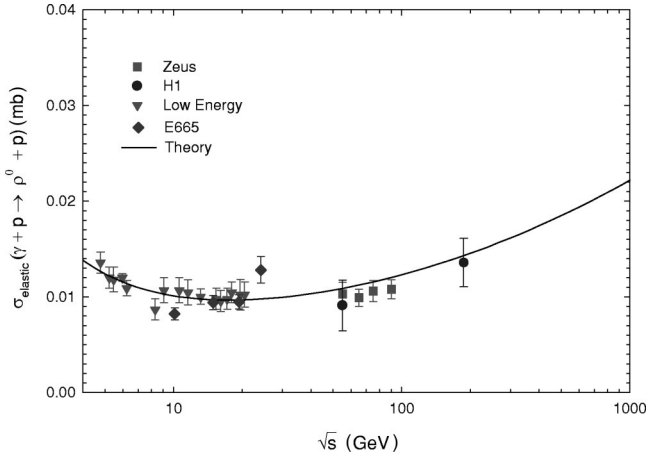

FIG. 10. The ''elastic'' photoproduction cross section, for the reaction $\gamma+p\rightarrow\rho^0+p$. The squares are Zeus data, the circles are H1 data, the diamond is E665, and the inverted triangles the low energy data.

We note that the results for ρ and B are very critical to our analysis. We have assumed that, in some manner, the gluons are related to the quarks. For a two quark system, such as the photon, the factors of 2/3 multiplying a cross section and $\sqrt{3/2}$ multiplying μ are the same for gluon-gluon as for quark-quark. If we relax this assumption and only use these factors in the quark, we get a sharp disagreement with our predicted ρ value, being considerably larger than the Compton value. The problem is further exacerbated in the predictions for B, with slopes from 11 GeV^{-2} (at 5 GeV) to 16 GeV^{-2} (at 80 GeV), which are much larger than the experimental values. This clearly has implications for constituent dynamics, which we will discuss further on.

To calculate the elastic cross sections $\sigma^{Vp}_{elastic}$ and differential cross sections $d\sigma^{Vp}/dt$ as a function of energy, we use

$$\sigma^{Vp}_{elastic}(s)=P^{Vp}_{had}\int |1-e^{i\chi^{\gamma p}(b,s)}|^2\, d^2\vec{b}, \qquad (7)$$

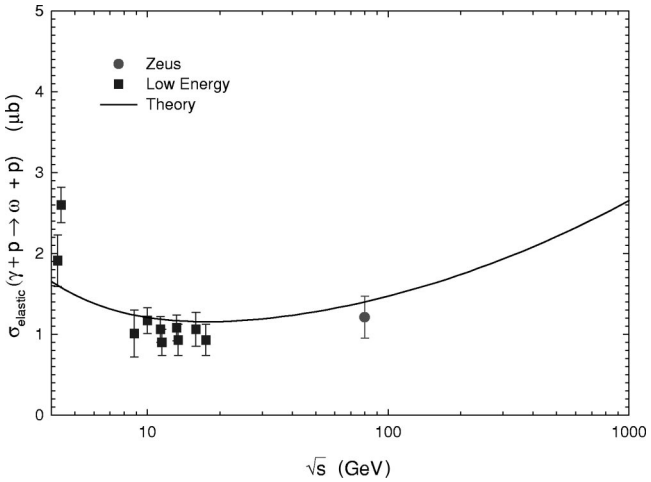

FIG. 11. The ''elastic'' photoproduction cross section for the reaction $\gamma+p\rightarrow\omega^0+p$. The circles are Zeus data, and the squares are the low energy data.

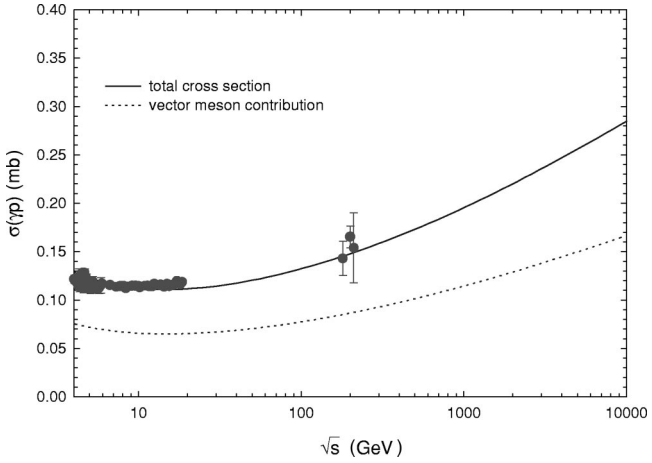

FIG. 12. The total ''elastic'' photoproduction cross section (dotted line), i.e., the sum of $\gamma+p\rightarrow\rho^0+p$, $\gamma+p\rightarrow\omega^0+p$, and $\gamma+p\rightarrow\phi^0+p$. For comparison we also show the total photoproduction cross section (solid line) along with the data.

where P_{had}^{Vp} is the appropriate probability for a photon to turn into V, with $V=\rho,\omega$ or ϕ. The differential scattering cross section is given by

$$\frac{d\sigma^{Vp}}{dt}(s,t)=\frac{P_{had}^{Vp}}{4\pi}\left|\int J_0(qb)(1-e^{i\chi^{\gamma p}(b,s)})\,d^2\vec{b}\right|^2, \quad (8)$$

where $t=-q^2$.

Since we normalize our data to the cross section found with $\chi^{\gamma p}$, and not to $(\sigma_{tot}^{\pi^+}+\sigma_{tot}^{\pi^-})/2$, we must multiply all $f_V^2/4\pi$ by 1.65. Hence, our effective couplings are $f_{\rho\ \mathrm{eff}}^2/4\pi=3.6$, $f_{\omega\ \mathrm{eff}}^2/4\pi=38.9$, and $f_{\phi\ \mathrm{eff}}^2/4\pi=30.4$.

Our evaluation of the ''elastic'' cross section for the reactions $\gamma+p\rightarrow\rho^0+p$ and $\gamma+p\rightarrow\omega^0+p$ is shown in Figs. 10 and 11, respectively. In Fig. 12 we sum all of our predictions for the elastic vector interactions for ρ, ω and ϕ and divide this sum by the ratio of $\sigma_{elastic}/\sigma_{tot}$. We find that the fraction of the total cross section for γp reactions that is contributed by the three light vector mesons (ρ, ω and ϕ) is ≈ 0.60. The remaining fraction can be made up of a mixture of heavier vector meson states and continuum states.

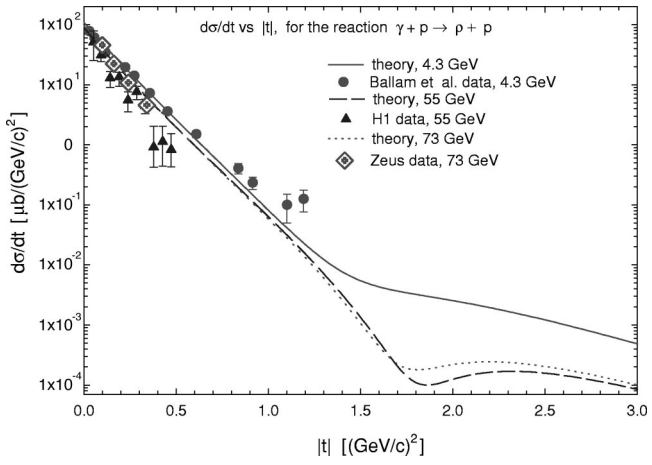

FIG. 13. The differential cross section for the ''elastic'' reaction $\gamma+p\rightarrow\rho^0+p$. The solid curve and the circles date of (data of Ballam *et al.*) are at $\sqrt{s}=4.3$ GeV, the dashed curve and triangles (H1 data) are at $\sqrt{s}=55$ GeV, and the dotted curve and diamonds are at $\sqrt{s}=73$ GeV (Zeus data).

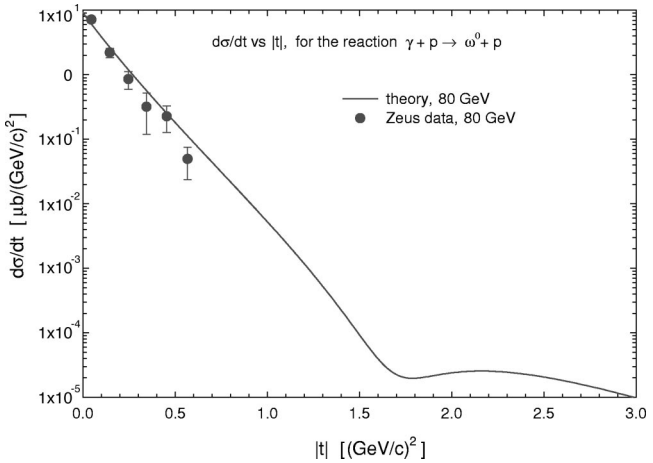

FIG. 14. The differential cross section for the ''elastic'' reaction $\gamma+p\rightarrow\omega^0+p$ at $\sqrt{s}=80$ GeV. The circles are the Zeus data.

The differential cross section, $d\sigma/dt$, for the ''elastic'' reactions $\gamma+p\rightarrow\rho^0+p$, $\gamma+p\rightarrow\omega^0+p$ and $\gamma+p\rightarrow\phi^0+p$ is plotted in Figs. 13, 14, and 15, respectively. The agreement, in absolute normalization and shape, of our results for all three light vector mesons with the experimental data for all available energies reinforces our confidence in the model.

IV. PHOTON-PHOTON INTERACTIONS

In this section, we consider $\gamma\gamma$ interactions. As was done for γp interactions, we will start from the eikonal $\chi^{\gamma p}(s,b)$ and multiply every cross section by 2/3 and multiply each μ by $\sqrt{3/2}$. Therefore,

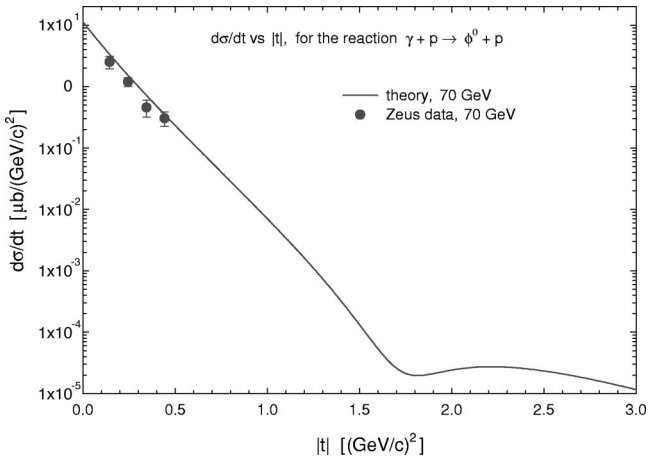

FIG. 15. The differential cross section for the ''elastic'' reaction $\gamma+p\rightarrow\phi^0+p$ at $\sqrt{s}=70$ GeV. The circles are the Zeus data.

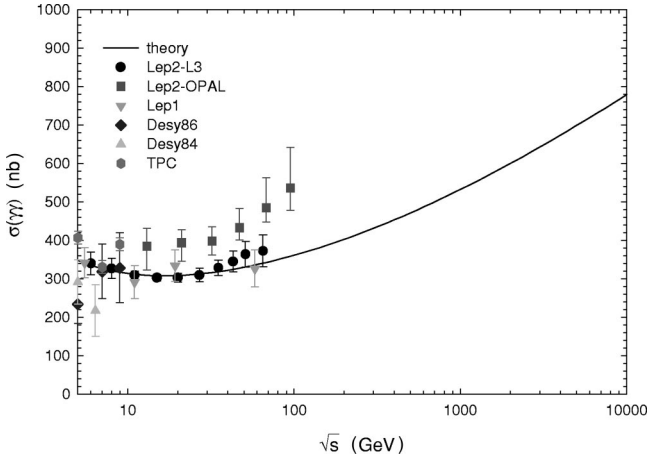

FIG. 16. The total cross section for $\gamma\gamma$ scattering. The data sources are indicated in the legend.

$$\chi^{\gamma\gamma}(s,b) = i[\tfrac{4}{9}\sigma_{qq}(s)W(b;\tfrac{3}{2}\mu_{qq}) + \tfrac{4}{9}\sigma_{qg}(s)W(b;\tfrac{3}{2}\sqrt{\mu_{qq}\mu_{gg}}) + \tfrac{4}{9}\sigma_{gg}(s)W(b;\tfrac{3}{2}\mu_{gg})]. \quad (9)$$

Using vector dominance we obtain

$$\sigma_{tot}^{\gamma\gamma}(s) = 2P_{had}^2 \int \{1 - e^{-\chi_I^{\gamma\gamma}(b,s)}\cos[\chi_R^{\gamma p}(b,s)]\}\, d^2\vec{b}, \quad (10)$$

where $P_{had} = 1/240$ is the probability that a photon will interact as a hadron. In Fig. 16 we plot our results for $\sigma_{tot}^{\gamma\gamma}(s)$ as a function of the energy, and compare it to the various sets of experimental data.

We also make predictions for ''elastic'' $\gamma\gamma$ reactions, in which both photons turn into vector mesons, and then elastically scatter off of each other, i.e., $\gamma + \gamma \to V_i + V_j \to V_i + V_j$, where $V_i, V_j = \rho, \omega, \phi$. We consider here 6 reactions:

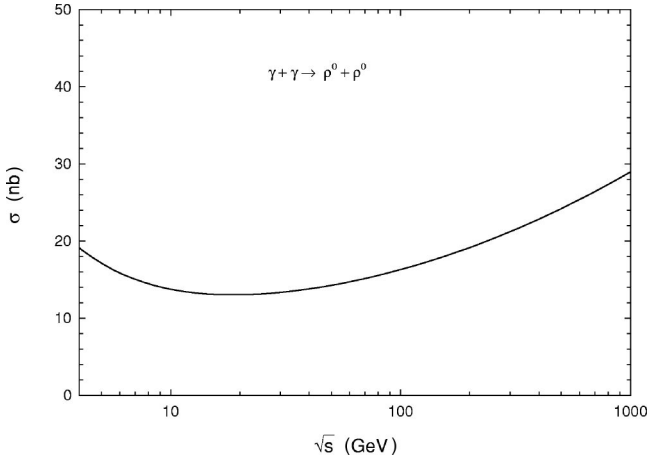

FIG. 17. The cross section for the ''elastic'' reaction $\gamma + \gamma \to \rho^0 + \rho^0$.

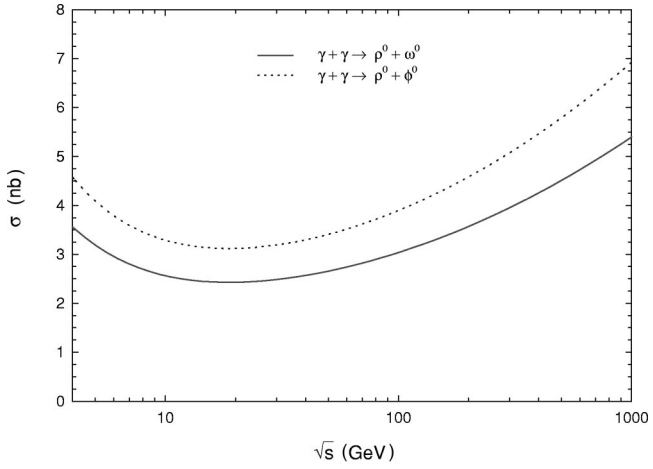

FIG. 18. The cross section for ''elastic'' $\gamma\gamma$ reactions. The solid curve is for the reaction $\gamma + \gamma \to \rho^0 + \omega^0$, and the dotted curve for $\gamma + \gamma \to \rho^0 + \phi^0$.

$$\gamma+\gamma\to\rho^0+\rho^0 \quad \gamma+\gamma\to\rho^0+\omega^0$$

$$\gamma+\gamma\to\rho^0+\phi^0 \quad \gamma+\gamma\to\omega^0+\omega^0$$

$$\gamma+\gamma\to\omega^0+\phi^0 \quad \gamma+\gamma\to\phi^0+\phi^0.$$

No data exist for these reactions, but they may be obtained at LEP in the foreseeable future. The total ''elastic'' scattering cross sections are calculated using the eikonal $\chi^{\gamma\gamma}$ multiplied by the factors $P_{had}^{V_i} P_{had}^{V_j}$,

$$\sigma_{elastic}^{\gamma\gamma}(s) = 2\, P_{had}^{V_i} P_{had}^{V_j} \int |1 - e^{i\chi^{\gamma\gamma}(b,s)}|^2\, d^2\vec{b} \quad (\text{if } i \neq j) \quad (11)$$

$$= P_{had}^{V_i} P_{had}^{V_j} \int |1 - e^{i\chi^{\gamma\gamma}(b,s)}|^2\, d^2\vec{b} \quad (\text{if } i = j). \quad (12)$$

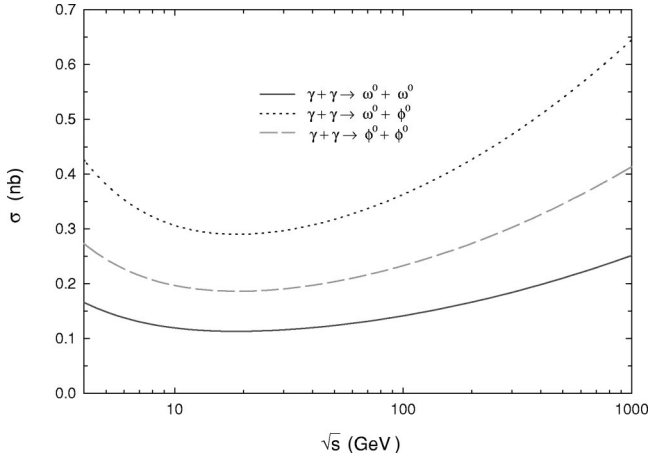

FIG. 19. The cross sections for $\gamma\gamma$ ''elastic'' reactions. The solid curve is for $\gamma + \gamma \to \omega^0 + \omega^0$, the dotted curve for $\gamma + \gamma \to \omega^0 + \phi^0$, and the dashed curve is for $\gamma + \gamma \to \phi^0 + \phi^0$.

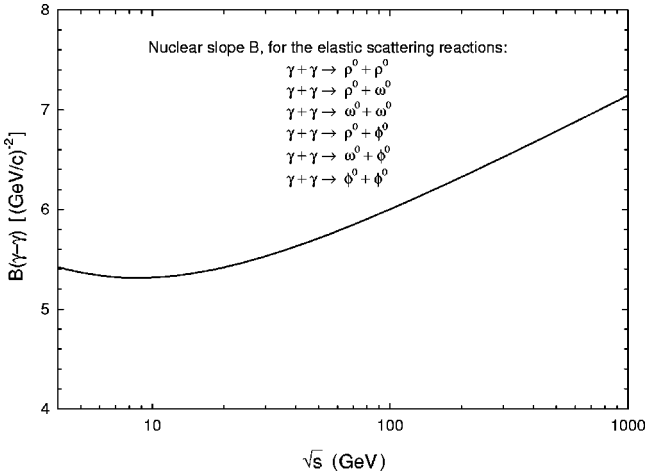

FIG. 20. The nuclear slope parameter for the ''elastic'' $\gamma\gamma$ reactions $\gamma+\gamma\rightarrow\rho^0+\rho^0$, $\gamma+\gamma\rightarrow\rho^0+\omega^0$, $\gamma+\gamma\rightarrow\omega^0+\omega^0$, $\gamma+\gamma\rightarrow\rho^0+\phi^0$, $\gamma+\gamma\rightarrow\omega^0+\phi^0$, and $\gamma+\gamma\rightarrow\phi^0+\phi^0$.

The factor of 2 takes into account that either photon could turn into a given vector meson.

We show in Figs. 17, 18, and 19 the energy dependence of these cross sections. The slopes are shown in Fig. 20. The slopes are, of course, the same for all elastic $\gamma\gamma$ reactions.

The differential cross section for the ''elastic'' $\gamma\gamma$ reactions is given by

$$\frac{d\sigma}{dt}(s,t)=2\,P_{had}^{V_i}\,P_{had}^{V_j}\frac{1}{4\pi}\left|\int J_0(qb)(1-e^{i\chi^{\gamma\gamma}(b,s)})\,d^2\vec{b}\right|^2$$

$$(\text{if } i\neq j) \tag{13}$$

$$=P_{had}^{V_i}\,P_{had}^{V_j}\frac{1}{4\pi}\left|\int J_0(qb)(1-e^{i\chi^{\gamma\gamma}(b,s)})\,d^2\vec{b}\right|^2$$

$$\text{if } i=j. \tag{14}$$

In Figs. 21–26 we show the differential cross section for these reactions for different center of mass $\gamma\gamma$ energies. Measuring the $|t|$ structure of the differential cross sections would be most interesting.

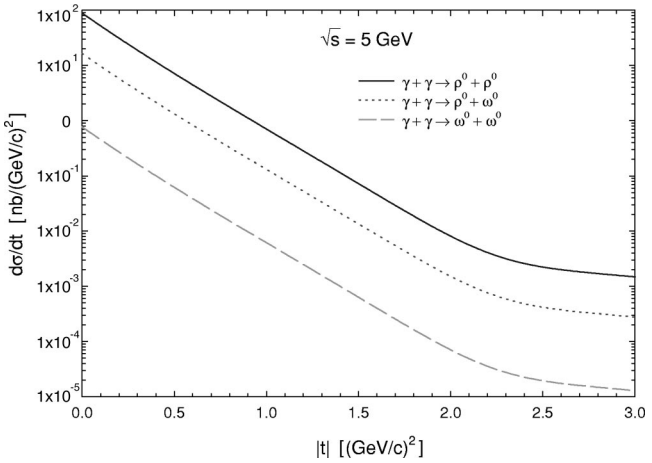

FIG. 21. The differential cross section for ''elastic'' $\gamma\gamma$ reactions at $\sqrt{s}=5$ GeV. The solid curve is for the reaction $\gamma+\gamma\rightarrow\rho^0+\rho^0$, the dotted curve for $\gamma+\gamma\rightarrow\rho^0+\omega^0$, and the dashed curve for $\gamma+\gamma\rightarrow\omega^0+\omega^0$.

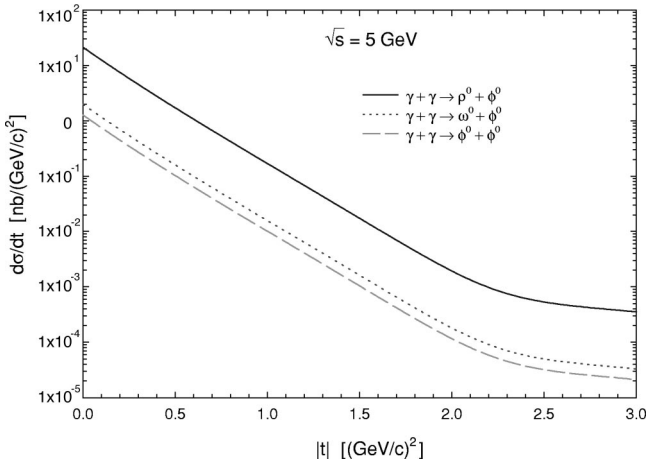

FIG. 22. The differential cross section for ''elastic'' $\gamma\gamma$ reactions at $\sqrt{s}=5$ GeV. The solid curve is for $\gamma+\gamma\rightarrow\rho^0+\phi^0$, the dotted curve for $\gamma+\gamma\rightarrow\omega^0+\phi^0$, and the dashed curve for $\gamma+\gamma\rightarrow\phi^0+\phi^0$.

V. SUMMARY AND CONCLUSIONS

Our conclusions for the total cross section for γp and $\gamma\gamma$ are summarized in Fig. 27. In order to scale nucleon-nucleon, γp, and $\gamma\gamma$ cross sections to a common curve, we have multiplied the γp cross sections by $1/P_{had}$ $(=240)$ and the $\gamma\gamma$ cross sections by $(1/P_{had})^2(=240^2)$. The nucleon-nucleon calculation is made using the even eikonal. For clarity, we have not included the Opal $\gamma\gamma$ experimental data. Basically, both the data and our theory approximately satisfy the factorization $\sigma_{tot}^{nn\text{-}even}/\sigma_{tot}^{\gamma p}=\sigma_{tot}^{\gamma p}/\sigma_{tot}^{\gamma\gamma}$, an immediate consequence of the eikonal being much smaller then unity in the energy region considered (up to ≈ 2 TeV). $\chi\ll 1$ is consis-

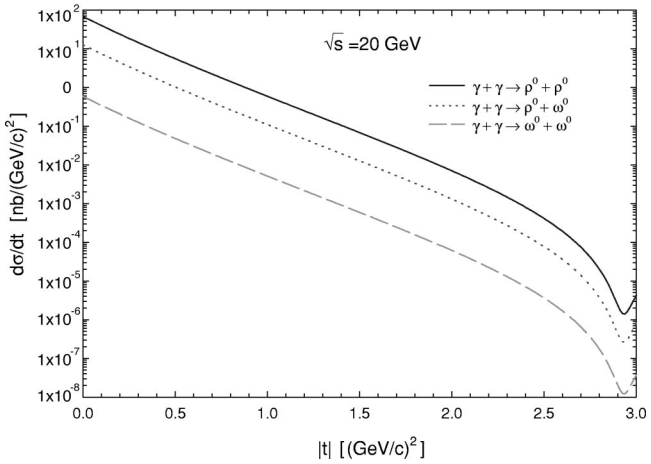

FIG. 23. The differential cross section for ''elastic'' $\gamma\gamma$ reactions at $\sqrt{s}=20$ GeV. The solid curve is for $\gamma+\gamma\rightarrow\rho^0+\rho^0$, the dotted curve for $\gamma+\gamma\rightarrow\rho^0+\omega^0$, and the dashed curve for $\gamma+\gamma\rightarrow\omega^0+\omega^0$.

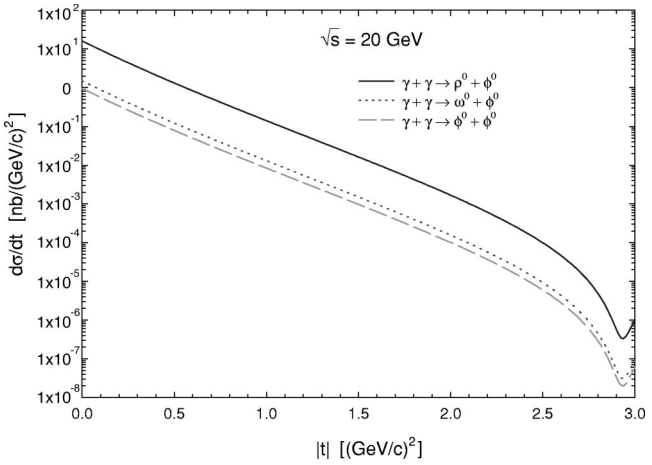

FIG. 24. The differential cross section for ''elastic'' $\gamma\gamma$ reactions at $\sqrt{s}=20$ GeV. The solid curve is for $\gamma+\gamma\rightarrow\rho^0+\phi^0$, the dotted curve for $\gamma+\gamma\rightarrow\omega^0+\phi^0$, and the dashed curve for $\gamma+\gamma\rightarrow\phi^0+\phi^0$.

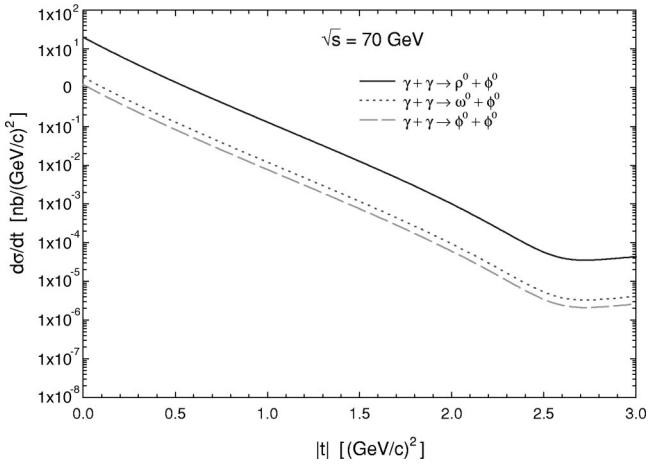

FIG. 26. The differential cross section for ''elastic'' $\gamma\gamma$ reactions at $\sqrt{s}=70$ GeV. The solid curve is for $\gamma+\gamma\rightarrow\rho^0+\phi^0$, the dotted curve for $\gamma+\gamma\rightarrow\omega^0+\phi^0$, and the dashed curve for $\gamma+\gamma\rightarrow\phi^0+\phi^0$.

tent with other evidences that the Tevatron energy is below ''Asymptopia.''

All data are in agreement with our QCD-inspired eikonal model which parametrizes the even eikonal. When appropriate quark counting factors and an energy independent factor $P_{had}=1/240$ are introduced, we can accommodate all γp data. With the same procedure we can describe the total $\gamma\gamma$ cross section. We stress that the γp and the $\gamma\gamma$ experimental data are consistent with P_{had} being energy independent, and with the factorization theorem.

We showed that VMD, combined with quark counting, fits all available ''elastic'' γp data. It correctly predicts the phase of the forward scattering amplitude for true Compton scattering, $\gamma+p\rightarrow\gamma+p$. Our model predicts that the three light vector mesons, ρ, ω and ϕ, account for roughly 60% of the total γp cross section.

Finally, our analysis suggests dynamical consequences. We pointed out that gluons are treated in the same footing as quarks. When we link the 2/3 factors exclusively to the quark composition of our eikonal, we get strong disagreement with the measured nuclear slope parameters B for γp ''elastic'' interactions, as well as disagreement between the ρ values that we predict for ''elastic'' scattering (such as $\gamma+p\rightarrow\rho^0+p$) and the dispersion relation calculation [18] for Compton scattering on a proton, $\gamma+p\rightarrow\gamma+p$.

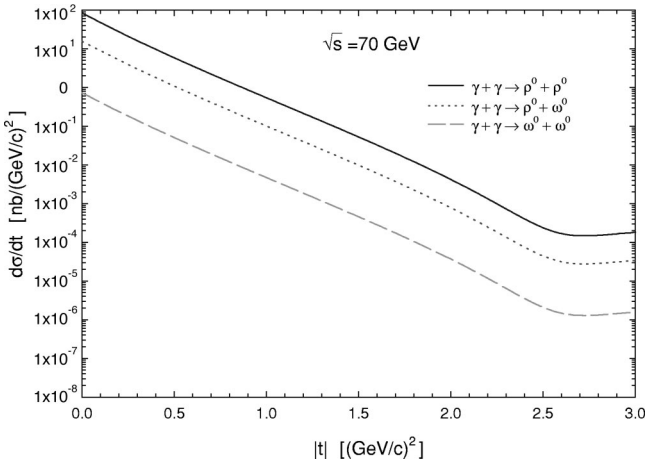

FIG. 25. The differential cross section for ''elastic'' $\gamma\gamma$ reactions at $\sqrt{s}=70$ GeV. The solid curve is for $\gamma+\gamma\rightarrow\rho^0+\rho^0$, the dotted curve for $\gamma+\gamma\rightarrow\rho^0+\omega^0$, and the dashed curve for $\gamma+\gamma\rightarrow\omega^0+\omega^0$.

ACKNOWLEDGMENTS

This work was supported in part by the Fundação de Amparo à Pesquisa do Estado de São Paulo (FAPESP), in part by the U.S. Department of Energy under Grants No. DA-AC02-76-Er02289 and No. DE-FG02-95ER40896, and in part by the University of Wisconsin Research Committee

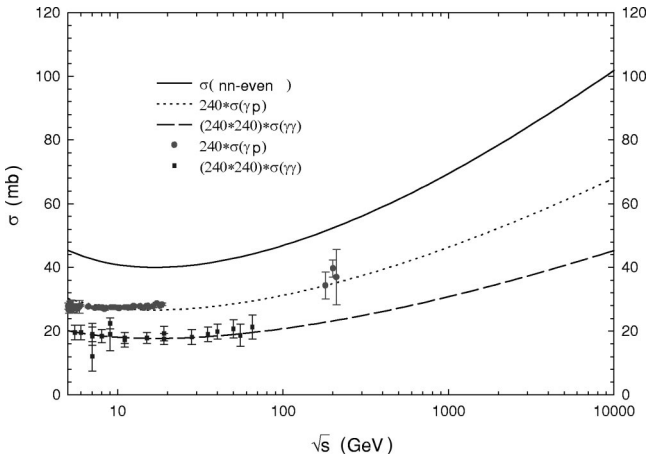

FIG. 27. The solid curve is the fitted total cross section for nucleon-nucleon scattering, using the even eikonal. The dotted curve is the predicted total cross section for γp scattering multiplied by $1/P_{had}$ $(=240)$. The circles are the γp data multiplied by $1/P_{had}$. The dashed curve is the predicted total cross section for $\gamma\gamma$ scattering multiplied by $(1/P_{had})^2(=240^2)$. The squares are $\gamma\gamma$ total cross section data multiplied by $(1/P_{had})^2$.

with funds granted by the Wisconsin Alumni Research Foundation.

APPENDIX A: EIKONAL FORMULATION

In order to ensure unitarity, we introduce the eikonal formalism in the two-dimensional transverse impact parameter space $\vec{b}$. We use the complex analytic eikonals, $\chi_{pp}(b,s)=\chi^{even}(b,s)-\chi^{odd}(b,s)$ and $\chi^{-}_{pp}(b,s)=\chi^{even}(b,s)+\chi^{odd}(b,s)$, even or odd under the transformation $E\rightarrow -E$ where E is the proton laboratory energy. This work largely follows the procedures and conventions used by Block and Cahn [14]. We write the center-of-mass differential elastic scattering cross section $d\sigma/d\Omega_{c.m.}$, the invariant differential elastic scattering distribution $d\sigma/dt$ and the total cross section σ_{tot} in terms of the center of mass scattering amplitude $f_{c.m.}$ as

$$\frac{d\sigma}{d\Omega_{c.m.}}=|f_{c.m.}|^2, \tag{A1}$$

$$\frac{d\sigma}{dt}=\frac{\pi}{k^2}|f_{c.m.}|^2, \tag{A2}$$

$$\sigma_{tot}=\frac{4\pi}{k}\mathrm{Im}f_{c.m.}(\theta=0), \tag{A3}$$

where k is the center of mass system momentum, θ is the center of mass system scattering angle, and $t=-2k^2(1-\cos\theta)$ is the invariant four-momentum transfer. The center of mass scattering amplitude [14] is given by

$$f_{c.m.}(s,t)=\frac{k}{\pi}\int e^{i\vec{q}\cdot\vec{b}}a(b,s)\,d^2\vec{b}, \tag{A4}$$

where $a(b,s)$ is the scattering amplitude in impact parameter space, $d^2\vec{b}=2\pi b\,db$, and $\vec{q}$ is a two-dimensional vector in impact parameter space $\vec{b}$ such that $q^2=-t$. Our complex eikonal, $\chi(b,s)=\chi_R(b,s)+i\chi_I(b,s)$, is defined so that the complex scattering amplitude in impact parameter space b is given by

$$a(b,s)=\frac{i}{2}(1-e^{-\chi_I(b,s)+i\chi_R(b,s)}). \tag{A5}$$

Using the optical theorem, $\sigma_{tot}(s)=4\pi\,\mathrm{Im}\{f_{c.m.}(s,0)\}/k$, the total cross section is given by

$$\sigma_{tot}(s)=2\int\{1-e^{-\chi_I(b,s)}\cos[\chi_R(b,s)]\}\,d^2\vec{b}, \tag{A6}$$

where we used Eq. (A4) evaluated in the forward direction ($t=0$). From Eq. (A2), we can evaluate the elastic scattering cross section as

$$\begin{aligned}\sigma_{elastic}(s)&=\frac{\pi}{k^2}\int|f_{c.m.}(s,t)|^2\,dt\\&=\frac{1}{k^2}\int|f_{c.m.}(s,t)|^2\,d^2\vec{q}\\&=\frac{1}{\pi^2}\int\int\int e^{i\vec{q}\cdot(\vec{b}-\vec{b}')}a(b,s)\\&\quad\times a^*(b',s)\,d^2\vec{q}\,d^2\vec{b}\,d^2\vec{b}'\\&=\frac{(2\pi)^2}{\pi^2}\int\int a(b,s)a^*(b',s)\,\delta^2(\vec{b}-\vec{b}')\,d^2\vec{q}\,d^2\vec{b}\\&=4\int|a(b,s)|^2\,d^2\vec{b}\\&=\int|1-e^{-\chi_I(b,s)+i\chi_R(b,s)}|^2\,d^2\vec{b}.\end{aligned} \tag{A7}$$

Thus, the inelastic cross section, defined as $\sigma_{tot}(s)-\sigma_{elastic}(s)$, is given by

$$\sigma_{inelastic}(s)=\int\{1-e^{-2\chi_I(b,s)}\}\,d^2\vec{b}. \tag{A8}$$

A convenient way of calculating the differential elastic scattering cross section is to introduce an integral representation of J_0 [see Eq. (9.1.18) of Ref. [19]],

$$J_0(z)=\frac{1}{2\pi}\int_0^{2\pi}e^{iz\cos\phi}\,d\phi, \tag{A9}$$

and rewrite Eq. (A4) as

$$\begin{aligned}f_{c.m.}(s,t)&=2k\int_0^\infty J_0(qb)\,a(b,s)b\,db\\&=\frac{k}{\pi}\int J_0(qb)\,a(b,s)\,d^2\vec{b}.\end{aligned} \tag{A10}$$

We can then write the differential scattering cross section as

$$\frac{d\sigma}{dt}(s,t)=\frac{1}{4\pi}\left|\int J_0(qb)(1-e^{-\chi_I(b,s)+i\chi_R(b,s)})\,d^2\vec{b}\right|^2. \tag{A11}$$

To calculate ρ, the ratio of the real to the imaginary part of the forward nuclear scattering amplitude, we write

$$\begin{aligned}\rho(s)&=\frac{\mathrm{Re}\{f_{c.m.}(s,0)\}}{\mathrm{Im}\{f_{c.m.}(s,0)\}}\\&=\frac{\mathrm{Re}\left\{i\int(1-e^{-\chi_I(b,s)+i\chi_R(b,s)})\,d^2\vec{b}\right\}}{\mathrm{Im}\left\{i\int(1-e^{-\chi_I(b,s)+i\chi_R(b,s)})\,d^2\vec{b}\right\}}.\end{aligned} \tag{A12}$$

The nuclear slope parameter is defined as

$$B(s)=\frac{d}{dt}\left[\ln\frac{d\sigma}{dt}(s,t)\right]_{t=0}. \tag{A13}$$

Expanding the exponential of Eq. (A4) around $q=0$ we get

$$f_{c.m.}(s,t)\propto\int\left[1+i\vec{q}\cdot\vec{b}-\frac{1}{2}(\vec{q}\cdot\vec{b})^2+\cdots\right]a(b,s)\,d^2\vec{b}. \tag{A14}$$

With this expansion and the definition of B we can eventually write the general expression for B as

$$B=\frac{\mathrm{Re}\left\{\int_0^\infty db\,b\,a(b,s)\int_0^\infty db\,b^3a^*(b,s)\right\}}{2\left|\int_0^\infty db\,b\,a(b,s)\right|^2}. \tag{A15}$$

If the phase of $a(b,s)$ is independent of b (this is the case when we either have a factorizable eikonal or an eikonal with a constant phase), this expression reduces to the more tractable form

$$B=\frac{\int_0^\infty db\,b^3a(b,s)}{2\int_0^\infty db\,b\,a(b,s)}=\frac{\int b^2a(b,s)\,d^2\vec{b}}{2\int a(b,s)\,d^2\vec{b}}. \tag{A16}$$

We note that B measures the size of the proton, i.e., B is related the average value of the square of the impact parameter b, weighted by $a(b,s)$. Introducing the eikonal, we find

$$B=\frac{1}{2}\frac{\int(1-e^{-\chi_I(b,s)+i\chi_R(b,s)})b^2\,d^2\vec{b}}{\int(1-e^{-\chi_I(b,s)+i\chi_R(b,s)})\,d^2\vec{b}}. \tag{A17}$$

The t dependence of the elastic differential cross section is described at small $|t|$ as

$$\begin{aligned}\frac{d\sigma}{dt}(s,t)&=\left|\frac{d\sigma}{dt}(s,t)\right|_{t=0}e^{Bt+Ct^2+\cdots}\\&=\left|\frac{d\sigma}{dt}(s,t)\right|_{t=0}\left[1+Bt+\left(\frac{B^2}{2}+C\right)t^2+\cdots\right].\end{aligned} \tag{A18}$$

The curvature parameter C is given by

$$C=\frac{1}{32}\frac{\int(1-e^{-\chi_I(b,s)+i\chi_R(b,s)})b^4\,d^2\vec{b}}{\int(1-e^{-\chi_I(b,s)+i\chi_R(b,s)})\,d^2\vec{b}}-\frac{1}{16}\left[\frac{\int(1-e^{-\chi_I(b,s)+i\chi_R(b,s)})b^2\,d^2\vec{b}}{\int(1-e^{-\chi_I(b,s)+i\chi_R(b,s)})\,d^2\vec{b}}\right]^2, \tag{A19}$$

where it was assumed that the phase of the eikonal is independent of b [see Eq. (4.45) of Ref. [14]]. We see that the curvature C can be positive, negative, or zero, whereas the nuclear slope parameter B must be positive.

APPENDIX B: QCD-INSPIRED EIKONAL

The even QCD-inspired eikonal is given by the sum of three contributions: gluon-gluon, quark-gluon, and quark-quark. They are individually factorizable into a product of a cross section times an impact parameter space distribution function, i.e.,

$$\begin{aligned}\chi^{even}(s,b)&=\chi_{gg}(s,b)+\chi_{qg}(s,b)+\chi_{qq}(s,b)\\&=i[\sigma_{gg}(s)W(b;\mu_{gg})+\sigma_{qg}(s)W(b;\sqrt{\mu_{qq}\mu_{gg}})\\&\quad+\sigma_{qq}(s)W(b;\mu_{qq})],\end{aligned} \tag{B1}$$

where the impact parameter space distribution function

$$W(b;\mu)=\frac{\mu^2}{96\pi}(\mu b)^3K_3(\mu b) \tag{B2}$$

is normalized so that $\int W(b;\mu)d^2\vec{b}=1$. As a consequence of both factorization and the normalization chosen for the $W(b;\mu)$, it should be noted that

$$\int\chi^{even}(s,b)\,d^2\vec{b}=i[\sigma_{gg}(s)+\sigma_{qg}(s)+\sigma_{qq}(s)], \tag{B3}$$

so that $\sigma_{tot}^{even}(s)=2\mathrm{Im}\{i[\sigma_{gg}(s)+\sigma_{qg}(s)+\sigma_{qq}(s)]\}$, for small χ.

To model the gluon-gluon interaction after QCD, we write its cross section as

$$\sigma_{gg}(s)=C_{gg}\int\Sigma_{gg}\Theta(\hat{s}-m_0^2)F_{gg}(x_1,x_2)d\tau, \tag{B4}$$

where $\Sigma_{gg}=9\pi\alpha_s^2/m_0^2$ is the cross section scale, $\hat{s}=\tau s$, and $F_{gg}=\int\int f_g(x_1)g(x_2)\delta(\tau-x_1x_2)dx_1dx_2$. For a scaling parametrization of the gluon structure function $f_g(x)=N_g(1-x)^5/x^{1+\epsilon}$, we can carry out the integrations and explicitly express $\sigma_{gg}(s)$ as

$$\sigma_{gg}(s)=C'_{gg}\Sigma_{gg}N_g^2\sum_{i=0}^{5}\left\{\frac{a(i)-\dfrac{b(i)}{i-\epsilon}}{i-\epsilon}-\tau_0^{i-\epsilon}\left(\frac{a(i)-\dfrac{b(i)}{i-\epsilon}}{i-\epsilon}+\frac{b(i)}{i-\epsilon}\log(\tau_0)\right)\right\} \quad \text{(B5)}$$

where $C'_{gg}=C_{gg}/q$, $\tau_0=m_0^2/s$, $a(0)=-a(5)=-411/10$, $a(1)=-a(4)=-975/2$, $a(2)=-a(3)=-600$ and $b(0)=b(5)=-9$, $b(1)=b(4)=-225$, $b(2)=b(3)=-900$. The constant N_g is given by $N_g=\frac{1}{2}(6-\epsilon)(5-\epsilon)\cdots(1-\epsilon)/5!$. The normalization constant C'_{gg} and the threshold mass m_0 are parameters to be fitted.

We note that the high energy behavior of $\sigma_{gg}(s)$ is controlled by

$$\lim_{s\to\infty}\int_{m_0^2/s}^{1}d\tau F_{gg}(\tau)\sim\int_{m_0^2/s}^{1}d\tau\frac{-\log\tau}{\tau^{1+\epsilon}}\sim\left(\frac{s}{m_0^2}\right)^{\epsilon}\log\left(\frac{s}{m_0^2}\right), \quad \text{(B6)}$$

where $\epsilon>0$. The cutoff impact parameter b_c is given by $cW_{gg}(b_c;\mu_{gg})s^{\epsilon}\log(s)\sim 1$, where c is a constant. For large values of μb, we can now write it as $c'(\mu_{gg}b_c)^{3/2}e^{-\mu_{gg}b_c}s^{\epsilon}\log(s)\sim 1$, with c' another constant. Therefore,

$$b_c=\frac{\epsilon}{\mu_{gg}}\log\frac{s}{s_0}+O\left(\log\log\frac{s}{s'_0}\right). \quad \text{(B7)}$$

As long as $\epsilon>0$, we reproduce the Froissart bound from QCD arguments as we go to very high energies, i.e.

$$\sigma_{tot}=2\pi\left(\frac{\epsilon}{\mu_{gg}}\right)^2\log^2\frac{s}{s_0}. \quad \text{(B8)}$$

The usual Froissart bound coefficient of the $\log^2(s/s_0)$ term, $1/m_\pi^2=20$ mb, is now replaced by $(\epsilon/\mu_{gg})^2\sim 0.002$ mb. Note that μ_{gg} controls the size of the area occupied by the gluons inside the nucleon.

The quark-quark interaction is simulated by a constant cross section plus a Regge-even falling cross section. It can be approximated by

$$\sigma_{qq}(s)=\Sigma_{gg}\left(C+C_{Regge}^{even}\frac{m_0}{\sqrt{s}}\right), \quad \text{(B9)}$$

where C and C_{Regge}^{even} are constants to be fitted.

The quark-gluon interaction is simulated by

$$\sigma_{qg}(s)=\Sigma_{gg}C_{qg}^{log}\log\frac{s}{s_0}, \quad \text{(B10)}$$

where the normalization constant C_{qg}^{log} and the square of the energy scale in the logarithmic term s_0 are constants to be fitted.

The total even contribution is then written as

$$\chi_{even}=i\left\{\sigma_{gg}(s)W(b;\mu_{gg})+\Sigma_{gg}\left(C+C_{Regge}^{even}\frac{m_0}{\sqrt{s}}\right)W(b;\mu_{qq})+\Sigma_{gg}C_{qg}^{log}\log\frac{s}{s_0}W(b;\sqrt{\mu_{qq}\mu_{gg}})\right\}, \quad \text{(B11)}$$

and it can be made analytic by the substitution $s\to se^{-i\pi/2}$ (see the table on p. 580 of Ref. [14], along with Ref. [20]).

The odd eikonal, $\chi^{odd}(b,s)i=\sigma_{odd}W(b;\mu_{odd})$, accounts for the difference between pp and $p\bar{p}$, and must vanish at high energies. It can be written as [see Eq. (5.5b) of Ref. [14]]

$$\chi^{odd}(b,s)=C_{odd}\Sigma_{gg}\frac{m_0}{\sqrt{s}}e^{i\pi/4}W(b;\mu_{odd}) \quad \text{(B12)}$$

where the normalization constant C_{odd} is to be fitted.

[1] M.M. Block, R. Fletcher, F. Halzen, B. Margolis, and P. Valin, Phys. Rev. D **41**, 978 (1990).

[2] D. Cline, F. Halzen, and J. Luthe, Phys. Rev. Lett. **31**, 491 (1973); P. L'Heureux, B. Margolis, and P. Valin, Phys. Rev. D **32**, 1681 (1985); L. Durand and H. Pi, Phys. Rev. Lett. **58**, 303 (1987); Phys. Rev. D **40**, 1436 (1989); V. Innocente, A. Capella, and J.T.T. Van, Phys. Rev. B **213**, 81 (1988); B. Margolis *et al.*, *ibid.* **213**, 221 (1988); B.Z. Kopeliovich, N.N. Nikolaev, and I.K. Potashnikova, Phys. Rev. D **39**, 769 (1989); J.C. Collins and G.A. Ladinsky, *ibid.* **43**, 2847 (1991).

[3] R.S. Fletcher, T.K. Gaisser, and F. Halzen, Phys. Rev. D **45**, 377 (1992); **45**, 3279(E) (1992); Phys. Lett. B **298**, 442 (1993).

[4] PLUTO Collaboration, Ch. Berger *et al.*, Phys. Lett. **149B**, 421 (1984); TPC/2γ Collaboration, H. Aihara *et al.*, Phys. Rev. D **41**, 2667 (1990); MD-1 Collaboration, S.E. Baru *et al.*, Z. Phys. C **53**, 219 (1992); L3 Collaboration, M. Acciarri *et al.*, Phys. Lett. B **408**, 450 (1997); F. Wäckerle, Nucl. Phys. B (Proc. Suppl.) **71**, 381 (1999).

[5] S. Söldner-Rembold, in Proceedings of the ''ICHEP'98,'' Vancouver, 1998, Report FREIBURG-EHEP-98-06, 1998, hep-ex/9810011.

[6] M.M. Block, E.M. Gregores, F. Halzen, and G. Pancheri, Phys. Rev. D **58**, 017503 (1998).

[7] R.C. Hwa and M.S. Zahir, Phys. Rev. D **23**, 2539 (1981).

[8] O.J.P. Eboli, F. Halzen, and J.K. Mizukoshi, Phys. Rev. D **57**, 1730 (1998).

[9] E710 Collaboration, N. Amos *et al.*, Phys. Rev. Lett. **63**, 2784 (1989).
[10] CDF Collaboration, F. Abe *et al.*, Phys. Rev. D **50**, 5550 (1994).
[11] J. Orear, in Proceedings of the International Conference (7^{th} Blois Workshop) on Elastic and Diffractive Scattering — Recent Advances in Hadron Physics, Seoul, Korea, 1997.
[12] UA4 Collaboration, C. Augier *et al.*, Phys. Lett. B **316**, 448 (1993).
[13] E710 Collaboration, N. Amos *et al.*, Phys. Rev. Lett. **68**, 2433 (1992).
[14] M.M. Block and R.N. Cahn, Rev. Mod. Phys. **57**, 563 (1985).
[15] M.M. Block and R.N. Cahn, Phys. Lett. **149B**, 245 (1984).
[16] E710 Collaboration, N. Amos *et al.*, Phys. Rev. Lett. **61**, 525 (1988).
[17] T.H. Bauer *et al.*, Rev. Mod. Phys. **50**, 261 (1978).
[18] M. Damashek and F.J. Gilman, Phys. Rev. D **1**, 1319 (1970).
[19] *Handbook of Mathematical Functions*, edited by M. Abramowitz and I. A. Stegun (U.S. GPO, Washington, D.C., 1964).
[20] R. J. Eden, *High Energy Collisions of Elementary Particles* (Cambridge University Press, Cambridge, England, 1967).